Electrical Engineering
https://doi.org/10.1007/s00202-021-01329-y

ORIGINAL PAPER

# Performance evaluation of interphase transformers based on a new 48-pulse AC–DC converter for industrial applications

**Christel Enock Ghislain Ogoulola[1] · Angelo José Junqueira Rezek[1] · François-xavier Fifatin[2] · Robson Bauwelz Gonzatti[3] · José Policarpo Gonçalves de Abreu[1] · Maurício Campos Passaro[1] · Tales Cleber Pimenta[3] · Vinicius Zimmermann Silva[1] · Mauro José Renó Ferreira[1] · Hugo Oliveira Vilas Boas[1]**

Received: 11 January 2021 / Accepted: 27 May 2021


**Abstract**
This paper evaluates the performance of two arrangements of interphase transformers using a new AC–DC 48-pulse converter (SC-48P) for industrial applications with high currents in the order of hundreds of kiloamperes, so that consumers and other loads connected to the SC-48P electrical grid are not affected by the harmful effects caused by harmonic currents injected into the grid by converters. The prototype uses a 7.5° and 4 kVA-220/220 V three-phase phase-shifting autotransformer and two groups of 24-pulse converters, each containing two 2 kVA-220/180/180 V identical three-phase three-winding non-conventional transformers with four 6-pulse converter bridges connected in parallel. The methodology for calculating the inductance for each IPT is given using the mathematical formulation of AC currents established and processed using the MathCad software. Computational simulations in normal and degraded modes were conducted in MATLAB/Simulink to prove the prototype's performance in terms of harmonic distortion and reliability, considering only three operational scenarios. The SC-48P was experimentally tested using available laboratory resources to validate the research. The obtained results meet IEEE-519 requirements and confirm the viability and applicability of the proposed converter in industrial rectification systems in terms of power quality improvements.

**Keywords** Power quality improvement · Interphase transformers · Reliability in multi-pulse converter · Industrial rectification · Phase-shift transformers

## 1 Introduction

Electrical power supplied as a continuous current is necessary for industrial applications, such as smelting and aluminum extraction, producing chlorine, aircraft application systems, rocket propulsion systems and other applications [1–3]. AC–DC multi-pulse converters (MPCs) are used in these applications and are an essential interface when transmitting generated power to the load.

✉ Christel Enock Ghislain Ogoulola
christel@unifei.edu.br

[1] Institute of Electrical Systems and Energy, Federal University of Itajubá, BPS Avenue, 1303–P.O. Box 50–Zip code, 37500–903Itajubá, MG, Brazil

[2] Polytechnic School of Abomey-Calavi, University of Abomey-Calavi, Abomey-Calavi, Benin

[3] Institute of Systems Engineering and Information Technology, Federal University of Itajubá, Itajubá, MG, Brazil

The use of MPCs with nonlinear characteristics makes the AC line current of the grid and the DC load voltage differ significantly from the sine and constant wave, respectively, thus generating adverse effects on the power quality. For example, vibrations and overheating can occur in generators if the AC line currents of the MPCs contain a large number of harmonics [4].

In other words, AC–DC converters inject harmonic currents on both the AC and DC side, which cause a series of problems such as harmonic distortion in the electrical system buses, heating in the electrical machines, additional losses in cables and transformers, instability in the electrical control systems and interference in protective operational systems. Therefore, harmonic mitigation is necessary so that the supply grid can obtain AC currents that are essentially sinusoidal and for the DC load voltage to remain practically constant, thus eliminating harmonic pollution in the AC electric system and consequently eliminating the resulting problems, these would pose for end consumers of electrical power.

Published online: 18 June 2021

Many studies have been carried out over the past few years that use three main methods to improve the power quality from MPCs [5–11,13]. The first method focuses on increasing the numbers of output phases in the phase-shift transformer to improve the ability of harmonic reduction [5,7,8]. Using this method, one can simultaneously improve the AC current profile and the DC voltage and enhance the power quality on both AC and DC sides of the converter system. However, increasing the number of phases in a phase-shifting transformer can be complex and hard to design and manufacture since the taps calculated for the winding can be pretty small.

The second method uses an interphase reactor (IPR) with multiple taps in the DC link at the output of the 12-pulse converter (SC-12P) [9,14]. For example, if the double-tapped IPR with optimal parameters is used, The SC-12P can operate as a 24-pulse converter system (SC-24P) with a theoretical THD of the line current of around 7.6% under normal conditions. When the IPR has three taps, an auxiliary circuit (usually a single-phase diodes or thyristors rectifier) must be placed at the output of the secondary winding in the IPR so that the SC-12P can reach the 36-pulse converter system level (SC-36P). Although adjusting the number of taps in the IPR is one alternative way to increase the number of pulses in an AC–DC converter system, the current flowing in the load can be quite high, causing conduction losses and commutation problems in the diodes and thyristors bridges.

The third method considers installing an auxiliary circuit with active or passive components on the AC or DC side of the MPC [9,11,12]. In other words, the active auxiliary circuit regulates the current via the active components, thus controlling the output current of the AC–DC 6-pulse converters (SC-6P). Although active auxiliary circuits can reduce harmonic content, the MPCs containing active auxiliary circuits cannot reach the pulse number required for the output DC voltage. Using a passive auxiliary circuit can reduce the complexity of the design and the kVA rating of the phase-shifting transformer and simultaneously reduce the AC line current and DC voltage ripples to improve the ability to minimize harmonics economically [15].

Therefore, a converter system topology was highlighted in [15]. Basically, the structure comprises a SC-12P with an autotransformer connected in delta and a non-conventional IPR with an auxiliary single-phase diode rectifier in the DC link. The primary winding in the non-conventional IPR is employed in this topology with three taps, and the secondary winding is connected to a single-phase diode rectifier.

Compared with the topologies that use methods 1 and 2, the solution proposed in [15] can efficiently operate under normal conditions only as a 48-pulse converter system (SC-48P) for both the AC current and the DC voltage sides. However, this topology offers better performance in terms of the harmonic distortion in the AC line current and ripple reduction in DC voltage, compared to topological circuits developed in [5,7–9,14]; the SC-48P can suffer from maintenance problems, is complex to manufacture and may be somewhat unreliable. The latter constitutes a significant concern for very high current industrial applications if there are functional inadequacies or faults in the electrical lines in some parts of the used equipment. Furthermore, the semiconductors used in this topology need to be activated by a control unit, increasing costs while also making the system more complex.

In this paper, we have chosen to examine a new topology of SC-48P intended for industrial applications in order to deal with the reliability mentioned above, complexity and maintenance issues. The main problem with MPCs connected in parallel is that the 6-pulse converter bridges must share the same DC current to simultaneously reach the desired harmonic reduction in the AC current and a minimum ripple coefficient in the DC voltage. To meet the harmonic requirements of the proposed SC-48P, this paper evaluates the performance of two IPT configurations in terms of power quality improvement. The topology of the proposed SC-48P uses four $+7.5°$ three-winding non-conventional transformers connected in extended delta, a $7.5°$ phase-shifting autotransformer, and eight SC-6Ps connected in parallel. The proposed scheme provides the following advantages:

i) Ease of maintenance, being that the prototype is composed of three-winding identical transformer units, allowing for quick substitution in the event of failure and less required physical space.
ii) The proposed converter can effectively operate as a SC-24P to SC-12P (depending on the scenarios) in degraded mode offering more reliability compared to other already existing ones.
iii) According to the experiment results, the experimental efficiency of SC-48P topology is slightly improved $\left(\eta_{exp} \cong 99.13\%\right)$.
iv) The SC-48P proposed has the ability in achieving reduced input line current THD of 2.9% complying the requirements set by the IEEE-519 standard and improving the proposed system power quality.
v) Viability and more applicability in electrical drive applications in the petroleum sector, for instance, employed to drive high-powered fans, pumps and compressors on offshore platforms.

The detailed analysis of the proposed SC-48P is discussed in the following sections. Section 2 describes the topology of the SC-48P proposed here, detailing its wiring diagram, together with the two IPT configurations employed here. Section 3 presents theoretically the taps calculations for the $+7.5°$ non-conventional transformer and the $7.5°$ phase-

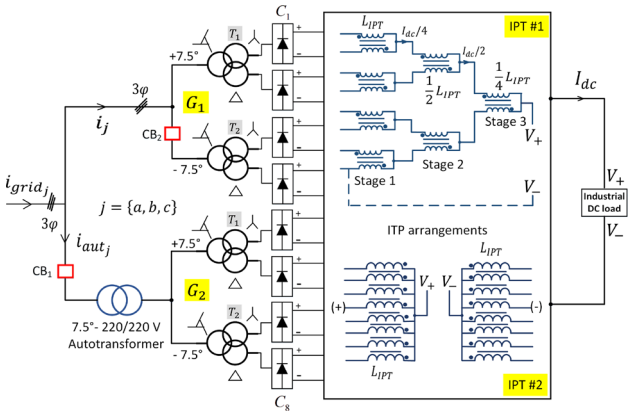


**Fig. 1** Topology of the proposed SC-48P system. $CB_1$ and $CB_2$ are three-phase circuit breakers

shifting autotransformer. Section 4 rigorously analyzes the theoretical AC currents in the SC-48P and its respective harmonic spectrum using the magnetomotive force (MMF) and Fourier series analysis. This was done using the MathCad software. Section 5 describes the methodology used to calculate the inductance value for each IPT. Section 6 presents the computational simulations of the SC-48P performed in MATLAB/Simulink evaluating the IPTs operating in both normal and degraded modes, in order to evaluate the performance of both IPTs in terms of the harmonic distortion in the AC current and the overall reliability of the supplied electrical energy. Section 7 studies the implementation of the devices at the laboratory using the available resources to verify the experimental results and to prove its viability and applicability for industrial application. Section 8 presents the conclusion of the study and offers suggestions for future studies in light of the findings presented here.

## 2 The structure of the proposed SC-48P

Fig1 shows the proposed topology of the SC-48P containing both arrangements of the IPTs.

In this figure, the SC-48P contains two identical SC-24P groups ($G_1$ and $G_2$), each containing two 2 kVA-220/180 V identical non-conventional three-phase three-winding transformers ($T_1$ e $T_2$) with a +7.5° extended delta configuration (ED-7.5°) in the primary winding, a 0°-wye winding (Wye-0°) in the secondary winding and a 30° delta winding (D-30°) in the tertiary winding.

Each transformer feeds two SC-6Ps connected in parallel. It is important to emphasize that if the SC-24P configuration is to be obtained, a transformer unit identical to $T_2$ must be used, and that it is possible to merely invert the feeder phase sequence of transformer $T_2$, which will thereby have a −7.5° extended delta in the primary winding, a 0° wye in the secondary winding and a 30° delta in the tertiary winding. Consequently, the phase shifting between the feeding secondary voltage at the converter bridges should be 15° and the harmonic characteristics of the input line current $i_j$ ($j = \{a, b, c\}$) of the SC-24P in group $G_1$ obey the generic relationship $h = 24 \cdot k \pm 1, k \in \mathbb{Z}_+$. Currents $i_j$, $i_{grid_j}$ and $i_{aut_j}$ are AC input line currents in group $G_1$, of the proposed SC-48P and of the autotransformer, respectively. The converters $C_i$ ($i = 1, 2 \cdots 8$) shown in Fig. 1 represent 6-pulse AC–DC three-phase converters.

On the other hand, the 7.5° and 4 kVA-220/220 V phase-shifting autotransformer is employed to allow for a phase shift of 7.5° between groups $G_1$ and $G_2$, thus obtaining the proposed SC-48P. The input line currents from the auto transformer $i_{aut_j}$ are phase-offset by 7.5° from currents $i_j$, making the harmonic characteristics of the line current at mains using the proposed SC-48P obey the generic relationship $h = 48 \cdot k \pm 1, k \in \mathbb{Z}_+$. Thus, the first harmonic characteristics in the current $i_{grid_j}$ for the proposed SC-48P are the 47th and 49th harmonics.

Due to the difference between the instantaneous DC output voltages of the converters bridge, an IPT is needed to support and absorb the difference and allow each SC-6P to operate independently. Therefore, two IPT arrangements are employed in this paper to evaluate its performance in the proposed SC-48P and in order to meet the requirements for less harmonic distortion in the AC current line of the power grid. The IPT inductance value in the first IPT arrangement (IPT #1) at each stage is designed to be half of the inductance value in the previous stage. The coupled group of inductors, marked (+) and (-), in the second IPT arrangement (IPT #2) are connected at the positive and negative poles at the outputs of the SC-48P bridge converters, respectively. We emphasize that the DC load is connected between $V_+$ and $V_-$ at the IPT output, as shown in Fig. 1.

The immediate advantage of the proposed SC-48P prototype is that it contains identical transformers, which is favorable from a maintenance standpoint. The proposed SC-48P also has other favorable applications for the aluminum industry, which requires very high service currents, which are in the order of hundreds of kiloamperes. The proposed converter system can effectively operate as a SC-24P and a SC-12P (this statement will be proven via computational simulations shown in Section. 6) in a degraded operational mode offering more reliability with respect to other topologies cited in existing scientific literature. In the context of modern industrial system applications, the proposed SC-48P prototype can also be favorable for highly reliable large-scale electrical drive applications (Fig. 2) in the petroleum sector, for example, employed to drive high-powered fans, pumps and compressors on offshore platforms [16].

In this topology, there is a traditional rectifier unit as a DC source for the supply of each three-phase group of H-bridge

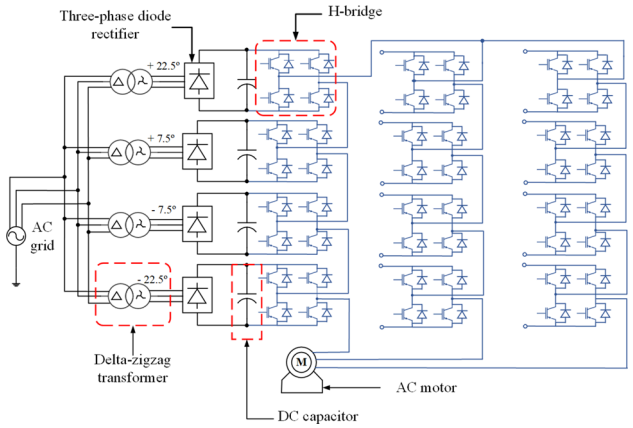


**Fig. 2** Recent application of special transformers for high-power converters and AC drives

connected in series for each phase of the AC electric motor. On the other hand, for instance, in situations of unavailability of a high voltage DC source with the necessary power to drive the prototypes employed by authors [17] and [18] (H-bridge multilevel inverter for improving THD and cascaded H-bridge multilevel cells, respectively), the proposed 48-pulse converter can be easily implemented and used to adjust the DC voltage at the input of the multilevel converter module.

## 3 Tap calculation for both the phase-shifting transformer and autotransformer

### 3.1 Tap calculation for the three-winding special transformer

Fig 3 shows the connection schematic of the transformer with ED in the primary winding. The different taps are calculated considering the displacement $\theta$ [19,20]. In Fig. 3, $aX_1$ and ab are the main and auxiliary coil voltage, respectively. The variables $N_1$, $N_2$ and $N_3$ represent the turns number related to the Wye (primary) and extended delta (secondary) winding, respectively. Based on triangle $aX_1X_3$ and applying the law of the sines, one can determine $aX_1$ and $aX_3$ via (1) and, consequently, taps $N_2$ and $N_3$.

$$\begin{cases} aX_1 = \dfrac{\sin(30^\circ - \theta)}{\sin(120^\circ)} \cdot X_1X_2 \\ aX_1 = \dfrac{\sin(30^\circ + \theta)}{\sin(120^\circ)} \cdot X_1X_2 \end{cases}. \tag{1}$$

If tap $aX_1X_3 = 100\%$ and $\theta = 7.5^\circ$, then: $aX_1 = 0.4419$ and $ac = aX_3 - cX_3 = aX_3 - cX_1$, from Eq. (1), i.e., $ac = 0.7029 - 0.4419 = 0.2610$. The transformer taps

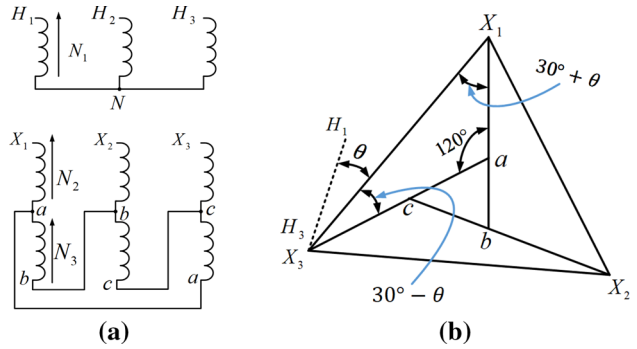


**Fig. 3** Transformer configuration with extended delta in the primary winding. **a** Connection diagram. **b** Phase diagram

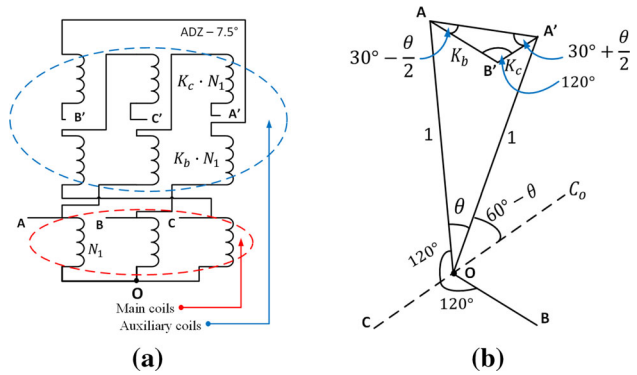


**Fig. 4** Autotransformer configuration. **a** Connection diagram. **b** Phase diagram

shown in Fig. 3 are equal to $N_2 = 44.19\%$ and $N_3 = 26.10\%$. For a 1:1 transformer relationship and $\theta = 7.5^\circ$, the 100% corresponds to $N_2 = 0.7653 \times N_1$ and $N_2 = 0.4520 \times N_1$.

### 3.2 Tap calculation for the three-phase phase-shifting autotransformer

Fig 4 shows the configuration of the +7.5° phase-shifting autotransformer with its phase diagram. It has one main coil and two auxiliary coils per phase [20].

Point "O" in Fig. 4 is the neutral point. The idea is to determine taps $K_b$ and $K_c$ mentioned in Fig. 4, to obtain the displacement $\theta$ between the input voltage $U_{OA}$ and the output voltage $U_{OA'}$ to form the SC-48P prototype. The value for $K_b$ and $K_c$ can be established for displacement $\theta$ by applying the law of the sines for triangle AOA' according to Eq. (2).

$$\begin{cases} K_b = \dfrac{2}{\sqrt{3}} \cdot \dfrac{\sin(\theta)}{\cos\left(\dfrac{\theta}{2}\right)} \cdot \sin\left(30^\circ + \dfrac{\theta}{2}\right) \\ K_c = \dfrac{2}{\sqrt{3}} \cdot \dfrac{\sin(\theta)}{\cos\left(\dfrac{\theta}{2}\right)} \cdot \sin\left(30^\circ - \dfrac{\theta}{2}\right). \end{cases} \tag{2}$$

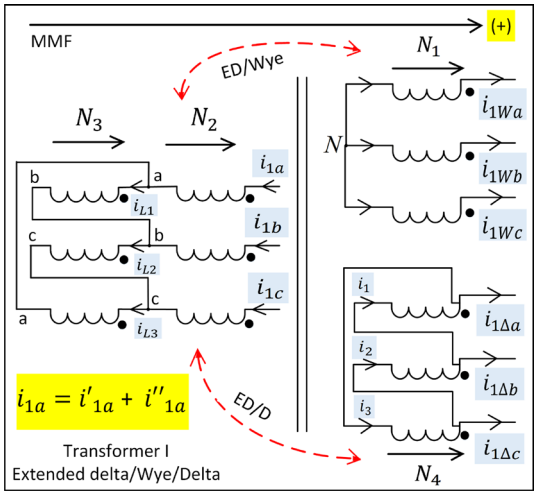


**Fig. 5** Schematic diagram of $T_1$ from group $G_1$

If $\theta = 7.5°$, one can obtain the taps required for the auto-transformer $K_b = 0.0839$ and $K_b = 0.0668$.

## 4 Theoretical analysis of the AC line currents in the proposed SC-48P

To theoretically evaluate the profile of the AC currents in the SC-48P and the respective harmonic content, mathematical analysis was carried out using the Fourier series and the MMF analysis. We assumed that the three-phase voltages and currents at the input of the converters bridges are totally balanced. The AC line current of the secondary and tertiary transformer winding connected in ED/Wye/D is equal to the inputs of each converter bridge. Fig 5 shows the schematic diagram of the special transformer $T_1$ from group $G_1$ as shown in Fig. 1.

The line currents $i_{1Wj}$ and $i_{1\Delta j}$ with $j = \{a, b, c\}$ are the input AC line currents for converter bridges $C_1$ and $C_2$. The (+) axis in Fig. 5 is the positive axis in the MMF analysis. For simplicity's sake, the AC line currents assume positive values when exiting the polarity markers on the coils and negative values when they enter. On the other hand, AC currents $i'_{1a}$ and $i''_{1a}$ are referred currents in the primary winding of transformer $T_1$ with ED/Wye and ED/D, respectively. We emphasize that the current calculations for the AC line currents established in this section were processed with the help of the MathCad software.

According to MMF analysis applied to each of the three phases $\left(\sum_j MMF_j = \sum_j (N \times i) = 0\right)$ [21], for connection ED/Wye shown in Fig. 5, one can establish the following system of equations according to (3).

$$\begin{cases} N_1 \cdot i_{1Wa}(\theta) - N_2 \cdot i'_{1a}(\theta) - N_3 \cdot i_{L1}(\theta) = 0 \\ N_1 \cdot i_{1Wb}(\theta) - N_2 \cdot i'_{1b}(\theta) - N_3 \cdot i_{L2}(\theta) = 0 \\ N_1 \cdot i_{1Wc}(\theta) - N_2 \cdot i'_{1c}(\theta) - N_3 \cdot i_{L3}(\theta) = 0 \end{cases} \tag{3}$$

where parameters $N_1$, $N_2$ and $N_3$ are the taps deduced in Section. 6 for a transformer ratio of 1:(180/220) and $\theta = \omega t$ is the angular frequency in radians. The AC line currents $i_{L1}$, $i_{L2}$ and $i_{L3}$ that flow through the auxiliary coils in the ED connection winding are calculated according to (4).

$$\begin{bmatrix} i_{L1}(\theta) \\ i_{L2}(\theta) \\ i_{L3}(\theta) \end{bmatrix} = \frac{1}{3} \cdot \begin{bmatrix} 1 & -1 & 0 & 1 \\ 0 & 1 & -1 & 1 \\ -1 & 0 & 1 & 1 \end{bmatrix} \times \begin{bmatrix} i'_{1a}(\theta) \\ i'_{1b}(\theta) \\ i'_{1c}(\theta) \\ 0 \end{bmatrix}. \tag{4}$$

Substituting (4) in (3), one obtains currents $i'_{1a}$, $i'_{1b}$ and $i'_{1c}$, in matrix form via Eq. (5).

$$\begin{bmatrix} i'_{1a}(\theta) \\ i'_{1b}(\theta) \\ i'_{1c}(\theta) \end{bmatrix} = \begin{bmatrix} \frac{N_2+p\cdot N_3}{N_1} & -p\cdot\frac{N_3}{N_1} & 0 \\ 0 & \frac{N_2+p\cdot N_3}{N_1} & -p\cdot\frac{N_3}{N_1} \\ -p\cdot\frac{N_3}{N_1} & 0 & \frac{N_2+p\cdot N_3}{N_1} \end{bmatrix}^{-1} \times \begin{bmatrix} i_{1Wa}(\theta) \\ i_{1Wb}(\theta) \\ i_{1Wc}(\theta) \end{bmatrix} \tag{5}$$

where $p = 1/3$. The input currents $i_{1Wa}$, $i_{1Wb}$ and $i_{1Wc}$ are calculated using the Fourier series analysis and can be expressed in Eq. (6).

$$\begin{cases} i_{1Wa}(\theta) = \frac{4}{\pi} \cdot I_d \cdot \sum_k \frac{1}{k} \cos\left(k \cdot \frac{\pi}{6}\right) \sin(k \cdot \theta) \\ i_{1Wb}(\theta) = \frac{4}{\pi} \cdot I_d \cdot \sum_k \frac{1}{k} \cos\left(k \cdot \frac{\pi}{6}\right) \sin\left(k \cdot \left(\theta - \frac{2\pi}{3}\right)\right) \\ i_{1Wc}(\theta) = \frac{4}{\pi} \cdot I_d \cdot \sum_k \frac{1}{k} \cos\left(k \cdot \frac{\pi}{6}\right) \sin\left(k \cdot \left(\theta + \frac{2\pi}{3}\right)\right) \end{cases} \tag{6}$$

where $k = 6 \cdot q \pm 1$ ($q \in \{0, 1 \cdots 8\}$), $k \in \mathbb{Z}_+$ e $I_{dc}$ are the harmonic order and the output DC current, respectively. The referred currents in the primary winding $i'_{1a}$, $i'_{1b}$ and $i'_{1c}$ for ED/Wye can be calculated in Eq. (7).

$$\begin{bmatrix} i'_{1a}(\theta) \\ i'_{1b}(\theta) \\ i'_{1c}(\theta) \end{bmatrix} = \begin{bmatrix} \alpha_1 & \beta_1 & \gamma_1 \\ \gamma_1 & \alpha_1 & \beta_1 \\ \beta_1 & \gamma_1 & \alpha_1 \end{bmatrix} \times \begin{bmatrix} i_{1Wa}(\theta) \\ i_{1Wb}(\theta) \\ i_{1Wc}(\theta) \end{bmatrix} \tag{7}$$

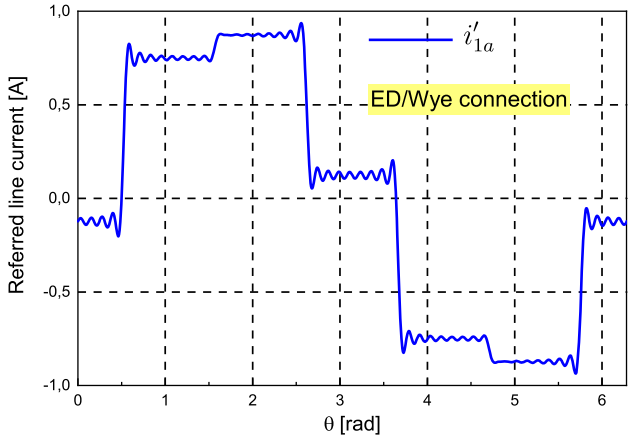


**Fig. 6** Waveform of AC line current $i'_{1a}$

where parameters $\alpha_1$, $\beta_1$ and $\gamma_1$ are the elements of inverse matrix established in Eq. (5) and are deduced according to Eq. (8).

$$\begin{cases} \alpha_1 = \dfrac{9N_1N_2^2 + 6N_1N_2N_3 + N_1N_3^2}{9N_2^3 + 9N_2^2N_3 + 3N_2N_3^2} \\ \beta_1 = \dfrac{N_1N_3^2 + 3N_1N_2N_3}{9N_2^3 + 9N_2^2N_3 + 3N_2N_3^2} \\ \gamma_1 = \dfrac{N_1N_3^2}{9N_2^3 + 9N_2^2N_3 + 3N_2N_3^2}. \end{cases} \tag{8}$$

Fig 6 shows the waveform of the referred current $i'_{1a}$ for phase A only, where $0 \leq \theta \leq 2{\cdot}\pi$ for an ED/Wye connection.

Using a similar procedure, AC line currents $i''_{1a}$, $i''_{1b}$ and $i''_{1c}$ can be established in Eq. (9), considering only an ED/D connection.

$$\begin{bmatrix} i''_{1a}(\theta) \\ i''_{1b}(\theta) \\ i''_{1c}(\theta) \end{bmatrix} = p \times \begin{bmatrix} \frac{N_2+p\cdot N_3}{N_1} & 0 & -p\cdot\frac{N_3}{N_1} \\ -p\cdot\frac{N_3}{N_1} & \frac{N_2+p\cdot N_3}{N_1} & 0 \\ 0 & -p\cdot\frac{N_3}{N_1} & \frac{N_2+p\cdot N_3}{N_1} \end{bmatrix}^{-1} \times \begin{bmatrix} i_{1\Delta a}(\theta) - i_{1\Delta b}(\theta) \\ i_{1\Delta b}(\theta) - i_{1\Delta c}(\theta) \\ i_{1\Delta c}(\theta) - i_{1\Delta a}(\theta) \end{bmatrix}. \tag{9}$$

The input currents $i_{1\Delta a}$, $i_{1\Delta b}$ and $i_{1\Delta c}$ are given according to Eq. (10) using the Fourier series analysis.

$$\begin{cases} i_{1\Delta a}(\theta) = \dfrac{4}{\pi}\cdot I_d \cdot \sum_k \dfrac{1}{k}\cos\left(k\cdot\dfrac{\pi}{6}\right)\sin\left(k\cdot\left(\theta - \dfrac{\pi}{6}\right)\right) \\ i_{1\Delta b}(\theta) = \dfrac{4}{\pi}\cdot I_d \cdot \sum_k \dfrac{1}{k}\cos\left(k\cdot\dfrac{\pi}{6}\right)\sin\left(k\cdot\left(\theta - \dfrac{\pi}{6} - \dfrac{2\pi}{3}\right)\right) \\ i_{1\Delta c}(\theta) = \dfrac{4}{\pi}\cdot I_d \cdot \sum_k \dfrac{1}{k}\cos\left(k\cdot\dfrac{\pi}{6}\right)\sin\left(k\cdot\left(\theta - \dfrac{\pi}{6} + \dfrac{2\pi}{3}\right)\right). \end{cases} \tag{10}$$

Consequently, the referred currents $i''_{1a}$, $i''_{1b}$, and $i''_{1c}$ can be given using Eq. (11).

$$\begin{bmatrix} i''_{1a}(\theta) \\ i''_{1b}(\theta) \\ i''_{1c}(\theta) \end{bmatrix} = p \times \begin{bmatrix} \alpha_2 & \beta_2 & \gamma_2 \\ \gamma_2 & \alpha_2 & \beta_2 \\ \beta_2 & \gamma_2 & \alpha_2 \end{bmatrix} \times \begin{bmatrix} i_{1\Delta a}(\theta) - i_{1\Delta b}(\theta) \\ i_{1\Delta b}(\theta) - i_{1\Delta c}(\theta) \\ i_{1\Delta c}(\theta) - i_{1\Delta a}(\theta) \end{bmatrix} \tag{11}$$

where parameters $\alpha_2$, $\beta_2$ and $\gamma_2$ are the elements of inverse matrix established in Eq. (9) and can be given according to Eq. (12).

$$\begin{cases} \alpha_2 = \dfrac{9N_4N_2^2 + 6N_4N_2N_3 + N_4N_3^2}{9N_2^3 + 9N_2^2N_3 + 3N_2N_3^2} \\ \beta_2 = \dfrac{N_4N_3^2 + 3N_4N_2N_3}{9N_2^3 + 9N_2^2N_3 + 3N_2N_3^2} \\ \gamma_2 = \dfrac{N_4N_3^2}{9N_2^3 + 9N_2^2N_3 + 3N_2N_3^2}. \end{cases} \tag{12}$$

The displacement between the secondary and tertiary windings is 30° due to the Wye/D connection. Therefore, tap $N_4$ in (12) is equal $\sqrt{3}\cdot N_1$. Fig 7 shows the waveform for the referred current $i''_{1a}$ only for phase A where $0 \leq \theta \leq 2\cdot\pi$ for an ED/D connection.

The input line currents $i_{1a}$, $i_{1b}$ and $i_{1c}$ of transformer $T_1$ from group from $G_1$ are given in Eq. (13).

$$\begin{cases} i_{1a}(\theta) = i'_{1a} + i''_{1a} \\ i_{1b}(\theta) = i'_{1b} + i''_{1b} \\ i_{1c}(\theta) = i'_{1c} + i''_{1c}. \end{cases} \tag{13}$$

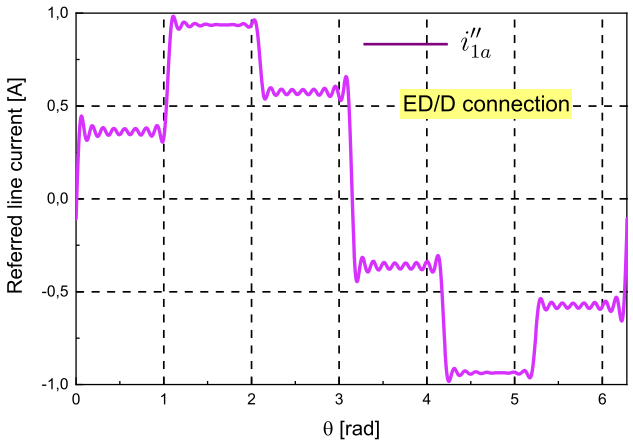


**Fig. 7** Waveform of AC line current $i''_{1a}$

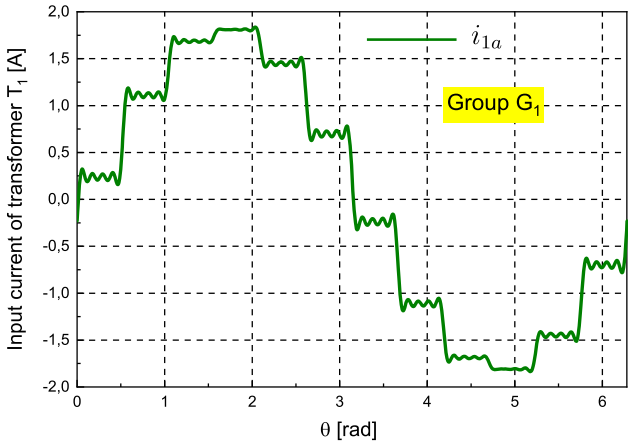


**Fig. 8** Waveform of AC line current $i_{1a}$

Figure 8 shows the waveform of AC line current $i_{1a}$ for $0 \leq \theta \leq 2 \cdot \pi$

An analogous process to the one previously described for obtaining the input line current $i_{1a}$ has been adopted here to determine the input AC line currents $i_{2a}$, $i_a$ and $i_{grid_a}$ for transformer $T_2$, of the SC-24P of the first group $G_1$ and of the supply grid of proposed SC-48P system, respectively. It is also worth noticing that the phase-shifting autotransformer was used in the proposed converter system shown in Fig. 1 to achieve a 7.5° displacement of between groups $G_1$ and $G_2$. Therefore, input line current $i_{aut_a}$ of the autotransformer is offset from line current $i_a$ by 7.5°. Figure 9 shows the AC line currents waveform $i_{2a}$, $i_a$ and $i_{grid_a}$ for $0 \leq \theta \leq 2 \cdot \pi$ .

Fig10 shows the harmonic content of AC line currents $i_a$ and $i_{grid_a}$ for the SC-24P and SC-48P, respectively. In this figure, only the first 50 harmonic components are considered. The fundamental AC line current was limited to 20% in order to make the harmonic components visible. The frequency range of 60 Hz to 3 kHz was considered for the THD calculation. The %THD of AC input grid current is computed using the relation between the rms and fundamental frequency component of the AC input line current. From the waveform shown in Fig. 9c, the rms value $I_{grid_{a,rms}}$ of AC input current $i_{grid_a}$ is calculated according to Eq. (14) using MathCad program.

$$I_{grid_{a,rms}} = \sqrt{\frac{1}{2\pi} \cdot \int_0^{2\pi} i^2_{grid_a}(\theta)\, d\theta}. \tag{14}$$

Similarly, the rms value of the fundamental component $I_{grid_{1a,rms}}$ $(k = 1)$ of the AC input line current $i_{grid_a}$ is obtained using Eq. (15).

$$I_{grid_{1a,rms}} = \sqrt{\frac{1}{2\pi} \cdot \int_0^{2\pi} i^2_{grid_{1a}}(\theta)\, d\theta}. \tag{15}$$

The effective values of the input line currents of the other phases are the same as those presented by expressions (14) and (15), since the mains system is considered balanced. Consequently, the theoretical THD value of AC input current is given according to Eq. (16).

$$\%THD_{i_{grid_a}} = \frac{\sqrt{I^2_{grid_{a,rms}} - I^2_{grid_{1a,rms}}}}{I_{grid_{1a,rms}}} = 2.94\%. \tag{16}$$

In Fig. 10, one can see that AC line currents $i_a$ and $i_{grid_a}$ have a THD equal to 6.60% and 2.94%, respectively. Therefore, the 23rd and 25th harmonics in the input line current of the power grid using the proposed SC-48P are eliminated. We emphasize that the harmonic content of AC input line current $i_{aut_a}$ of the autotransformer is similar to current $i_a$ of the SC-24P; however, the THD value is reduced due to the filtering effect of the phase-shifting autotransformer.

## 5 The method to determine the IPT inductance value for both IPTs

This section will deal with the inductance calculation for each of the IPT configurations for the proposed SC-48P shown in Fig. 1. We emphasize that usually the harmonic content is reduced when the IPT inductance value is increased. Therefore, to estimate the IPT inductance value, it is very important to meet the AC input line current requirements of the proposed SC-48P.

### 5.1 Method for estimating the IPT #2 inductance value

A calculation method using a configuration similar to the IPT #2 was proposed according to [22] to estimate the inductance

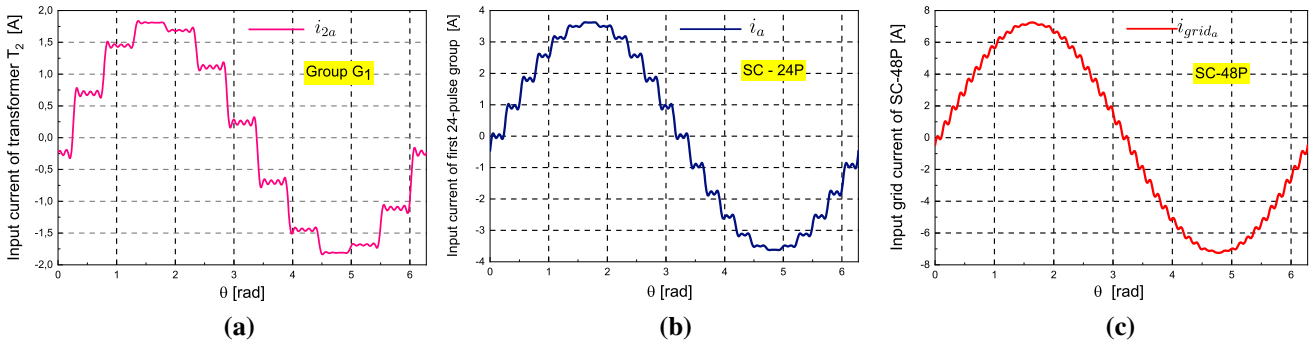


**Fig. 9** Waveform of the AC line currents. **a** AC line current $i_{2a}$. **b** AC line current $i_a$. **c** AC current grid $i_{grid_a}$

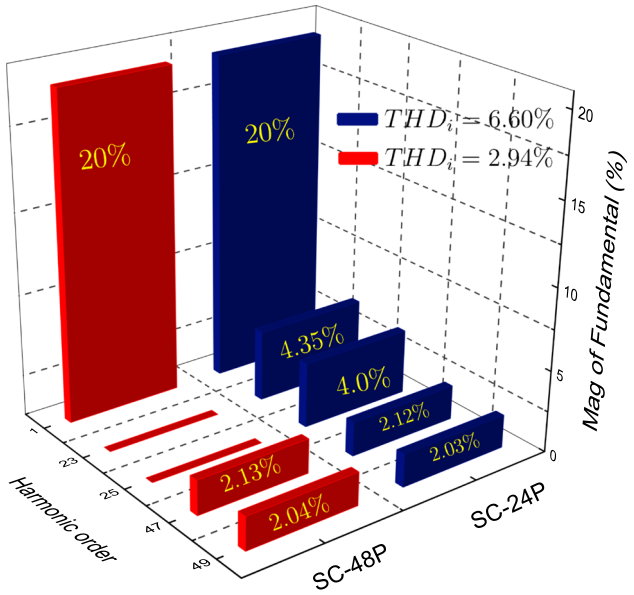


**Fig. 10** Harmonic spectrum of AC line currents $i_a$ and $i_{grid_a}$

values applied to an 18-pulse converter system (SC-18P). Thus, this method has been adopted here for the proposed SC-48P. Before estimating the IPT #2 inductance value, one must first establish the normalized reference parameters for the SC-48P.

$$V_{ref} = V_{1Wj} = V_{1\Delta j} = V_{2Wj} = V_{2\Delta j} = V_{3Wj} = V_{3\Delta j} = V_{4Wj} = V_{4\Delta j} \tag{17}$$

where $V_{ref}$, $V_{1Wj}$, $V_{1\Delta j}$, $V_{2Wj}$, $V_{2\Delta j}$, $V_{3Wj}$, $V_{3\Delta j}$, $V_{4Wj}$ and $V_{4\Delta j}$ ($j = \{a, b, c\}$) are the RMS phase to neutral input voltages for converter bridges and $V_{ref}$ is the reference voltage.

The reference power, frequency, current and impedance are given according to Eq. (18).

$$P_{ref} = \frac{P_{dc}}{24}, \quad f_{ref} = f_{grid}, \quad I_{ref} = \frac{P_{ref}}{V_{ref}} \quad \text{and} \quad Z_{ref} = \frac{V_{ref}^2}{P_{ref}} \tag{18}$$

where $P_{dc}$ and $f_{grid}$ are the nominal output power and the frequency grid of the proposed SC-48P, respectively. The normalized IPT #2 impedance value can be calculated using Eq. (19).

$$Z_{IPT-N} = \frac{Z_{IPT}}{Z_{ref}} = 2 \cdot \pi \underbrace{\frac{I_{ref} \cdot f_{ref}}{V_{ref}} \cdot L_{IPT}}_{L_{IPT-N}} = 2 \cdot \pi \cdot L_{IPT-N}. \tag{19}$$

The normalized IPT #2 inductance value can be deduced according to (20).

$$L_{IPT-N} = L_{IPT} \cdot \left( \frac{I_{ref} \cdot f_{ref}}{V_{ref}} \right). \tag{20}$$

The real IPT #2 inductance value is estimated in (21).

$$L_{IPT} = L_{IPT-N} \cdot \left( \frac{24 \cdot V_{1Wa}^2}{P_{dc} \cdot f_{grid}} \right). \tag{21}$$

The purpose of the presented method is to vary $L_{IPT-N}$ to achieve the smallest THD level possible. (This variation was made in a simulation). Figure 11 shows the THD variation versus normalized inductance $L_{IPT-N}$. We observe in Fig. 11 that normalized inductance values larger than 31 mH correspond to practically constant THD levels. Therefore, this value can be considered as an optimal value for estimating the

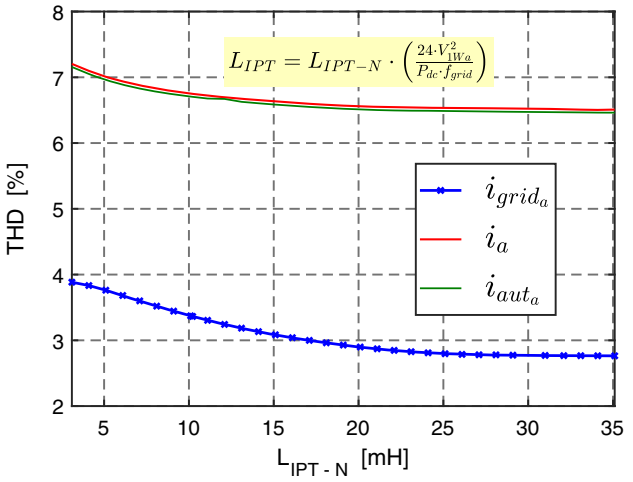


**Fig. 11** THD variation versus normalized inductance $L_{IPT-N}$ for AC line currents $i_{grid_a}$, $i_a$ and $i_{aut_a}$

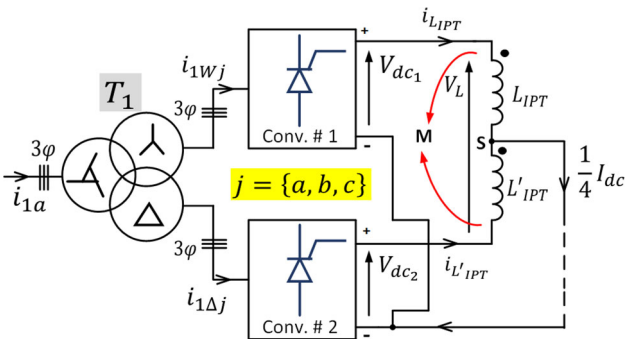


**Fig. 12** Extracted part of the proposed SC-48P system

real inductance of IPT #2. Consequently, if $V_{1Wa} = 103.92$ V (RMS value), $f_{grid} = 60$ Hz and $P_{dc} = 6.4$ kW (simulation value), then $L_{IPT} = 20.92$ mH.

## 5.2 Method for estimating the IPT #1 inductance value

To calculate the IPT #1 inductance value, we must first consider the analysis of an extracted part of the proposed SC-48P system illustrated in Fig. 12.

One can express the voltage $V_L$ over the interphase inductor using (22), where $L_{IPT} = L'_{IPT}$ and according to the procedure methodology established in [23].

$$V_L(\theta) = L_{IPT} \cdot \frac{d}{d\theta}\left(i_{L_{IPT}}(\theta) - i_{L'_{IPT}}(\theta)\right) + M \cdot \frac{d}{d\theta}\left(i_{L_{IPT}}(\theta) - i_{L'_{IPT}}(\theta)\right) \tag{22}$$

where $L_{IPT}, L'_{IPT}$ and $M$ are the inductances of the interphase inductors, and the mutual inductance, respectively. If $L_{IPT} \cong M$, Eq. (22) can be rewritten according to (23).

$$V_L(\theta) = 2 \cdot L_{IPT} \cdot \frac{d}{d\theta}\left(i_{L_{IPT}}(\theta) - i_{L'_{IPT}}(\theta)\right). \tag{23}$$

At node S in Fig. 12, results: $i_{L'_{IPT}}(\theta) = \frac{1}{4} \cdot I_{dc} - i_{L_{IPT}}(\theta)$. Thus, Eq. (23) can be rewritten in (24) assuming that current ripple $\left(\frac{1}{4} \cdot I_{dc}\right)$ is negligible in relation to the current ripple at bridges $i_{L_{IPT}}$ and $i_{L'_{IPT}}$.

$$V_L(\theta) = 4 \cdot L_{IPT} \cdot \frac{d}{d\theta}\left(i_{L_{IPT}}(\theta)\right). \tag{24}$$

Consequently, according to (24), the effective inductance value for IPT #1 is equal to four times the very own inductance value of each inductor. On the other hand, the voltage $V_L$ over the interphase inductor is equal to the difference between the instantaneous DC output voltages $V_{dc_1}$ and $V_{dc_2}$ at each 6-pulse converter bridge (Fig. 12) and can be given according to (25) by using the Fourier series analysis.

$$V_L(\theta) = \frac{12\sqrt{6}}{\pi} \cdot V_{1Wa} \cdot \sum_{k=1,2}^{\infty} \frac{1}{36k^2 - 1} \cdot \sin(6 \cdot k \cdot \theta). \tag{25}$$

Since the sixth harmonic ($k = 1$) is predominant in the output DC voltage in the SC-48P system for the simple reason that the converter bridges are connected in parallel, Eq. (25) can be rewritten as (26).

$$V_L(\theta) = \underbrace{\frac{12\sqrt{6}}{35 \cdot \pi} \cdot V_{1Wa}}_{V_{L_{peak}}} \cdot \sin(6 \cdot \theta). \tag{26}$$

The IPT #1 inductance value can be calculated using (27), which has equations equivalent to:

$$\begin{cases} I_{L_{IPT_{peak}}} = \dfrac{V_{L_{peak}}}{2\pi \cdot (6 \cdot f_{grid}) \cdot (4 \cdot L_{IPT})} \\ \Delta I_{L_{IPT}} = \dfrac{\Delta V_L}{2\pi \cdot (6 \cdot f_{grid}) \cdot (4 \cdot L_{IPT})} \end{cases} \tag{27}$$

where variables $V_{L_{peak}}$ is the voltage peak, $I_{L_{IPT_{peak}}}$ is the current peak, $\Delta V_L = 2 \cdot V_{L_{peak}}$ obtained in relation to the average voltage is the voltage ripple and $\Delta I_{L_{IPT}}$ is the current ripple. The inductances $L_{IPT}$ and $L'_{IPT}$ of the coupled

**Table 1** Simulation and experimental parameters. The units of the parameters are set to SI

| Components parameters | Transformer (ED–Wye–D) | Autotransformer |
|---|---|---|
| Primary resistance $(R_p)$ | 0.5206 $\Omega$ | 0.0762 $\Omega$ |
| Primary inductance $(L_p)$ | $3.402 \times 10^{-4}$ H | $8.634 \times 10^{-4}$ H |
| Secondary resistance $(R_s)$ | 0.5023 $\Omega$ | 0.0762 $\Omega$ |
| Secondary inductance $(L_s)$ | $6.317 \times 10^{-4}$ H | $8.634 \times 10^{-4}$ H |
| Tertiary resistance $(R_t)$ | 0.4207 $\Omega$ | – |
| Tertiary inductance $(L_t)$ | $5.2 \times 10^{-4}$ H | – |
| Magnetization resistance $(R_m)$ | 668.72 $\Omega$ | 1008.19 $\Omega$ |
| Magnetization inductance $(L_m)$ | 1.3247 H | 1.5314 H |
| Power grid and DC load specifications $(V_{grid}/L_{grid}/f_{grid}/P_{dc})$ | 220 V (line to line)/0.1 mH/60 Hz/6.4–2.978 kW | |

*Note that 80% and 37.23% of rated active power are considered as DC load power in the simulation model and implementation tests, respectively

inductors are arbitrarily calculated using maximum ripple equal to $\Delta I = 10\%$. (This value is usually specified by the designer). If the ripple amplitudes $\Delta I_{L_{IPT}}$ e $\Delta I_{L'_{IPT}}$ are equal, then:

$$\Delta I_{L_{IPT}} = \Delta I_{L'_{IPT}} = \frac{I_{dc} \cdot \Delta I}{8} = \frac{2 \cdot V_{L_{peak}}}{2\pi \cdot (6 \cdot f_{grid}) \cdot (4 \cdot L_{IPT})}. \tag{28}$$

Lastly, inductance value $L_{IPT}$ of IPT #1 for the proposed SC-48P is established according to Eq. (29).

$$L_{IPT} = \frac{72 \cdot V_{1Wa}^2}{35 \cdot \pi^3 \cdot f_{grid} \cdot P_{dc} \cdot \Delta I}. \tag{29}$$

If $P_{dc} = 6.4$ kW (simulation value), $f_{grid} = 60$ Hz, $\Delta I = 10\%$ and $V_{1Wa} = 103.92$ V, then the inductance value is approximately equal to $L_{IPT} = 18.66$ mH.

It is worth emphasizing that the IPT #1 configuration for the inductance value for each stage is designed to be half of the inductance value of the previous stage. Furthermore, the inductance values $L_{IPT}$, established and calculated using Eqs. (21) and (29) for IPT #2 and IPT #1, respectively, are specified in the computational simulations conducted in Sect. 6.

## 6 Simulation results of the proposed SC-48P for both IPT #1 and IPT #2 configurations

To evaluate the performance and efficiency of both the IPTs, the proposed SC-48P was modeled and simulated in MATLAB/Simulink. The tap values were calculated in Section. 3 for a 2 kVA-220/180 V transformer using an ED/Wye/D connection, considering only a 1:1 transformer ratio. Nonetheless, the prototype implemented had a transformer ratio of 1:(180/220), i.e., 1:0.82, and the taps were $N_2 = 0.9354 \times N_1$, $N_3 = 0.5524 \times N_1$ and $N_4 = 1.7320 \times N_1$ [20]. The 4 kVA-220/220 V three-phase phase-shifting autotransformer and the non-conventional transformer used in the proposed SC-48P converter were implemented in MATLAB/Simulink software based on the single-phase transformers available in the software library.

The inductance values of IPT, $L_{IPT}$ calculated in Section. 5 for both IPTs configurations are specified in the simulation model. The non-conventional transformer and the phase-shifting transformer parameters were acquired by conducting no load and short-circuit tests and are specified in the simulation model. A DC load type R-L, with a constant nominal rated power of 6.4 kW (simulation value), was considered the industrial load. The SC-6Ps bridges, as shown in Fig. 1, are diode bridge converters. The specifications of the simulated model are listed in Table 1.

It is noteworthy that there are many ways in which faults in electrical lines and/or equipment may occur when using the proposed SC-48P. Therefore, to evaluate and validate the reliability and applicability of the proposed SC-48P, only three scenarios were considered in the simulated model for each of the IPT configurations. Two three-phase circuit breakers, $CB_1$ and $CB_2$, as shown in Fig. 1, were employed to isolate the electrical line from faults.

i) The proposed SC-48P operating in normal mode ($CB_1$ and $CB_2$ closed), i.e., no faults registered when the special transformers and autotransformer are working;
ii) When the phase-shifting autotransformer is defective or taken out of the circuit ($CB_1$ open and $CB_2$ closed);
iii) When the autotransformer is defective or removed ($CB_1$ open) and a fault in the feeding phase in the first transformer $T_1$ from group $G_1$, consequently activating $CB_2$ (Fig. 1).

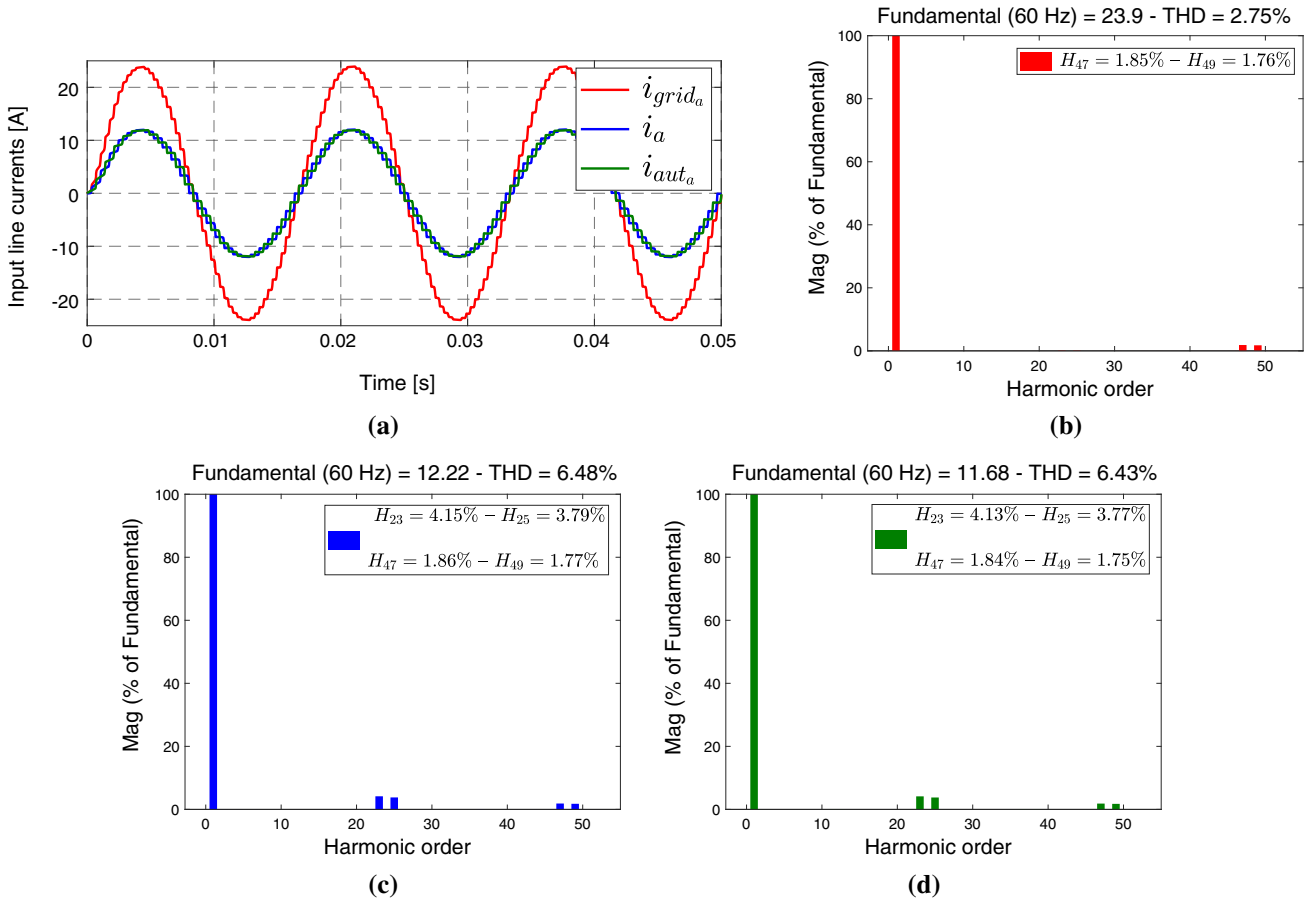


**Fig. 13** Simulation results of the proposed SC-48P operating under normal conditions for IPT #1. **a** Waveform of AC line currents $i_{grid_a}$, $i_a$ and $i_{aut_a}$. **b**, **c** and **d** Harmonic spectrum of currents $i_{grid_a}$, $i_a$ and $i_{aut_a}$, respectively

Fig 13 shows the results obtained for the proposed SC-48P operating under normal condition for an IPT #1.

One can see AC line currents for only phase A $i_{grid_a}$, $i_a$ and $i_{aut_a}$ have THDs equal to 2.75%, 6.48% and 6.43% (meeting the IEEE-519 requirements [24]), respectively, in relation to the fundamental AC component. All of the amplitudes for the harmonics are mentioned. One can also see the presence of the 47th and 49th harmonics in AC grid current and the profile of $i_{grid_a}$ is practically sinusoidal. It should be noted that there is a small difference between the value obtained for the THD levels in currents $i_a$ and $i_{aut_a}$. This difference, as mentioned in Section. 4, is due to the filtering effect of three-phase phase-shifting autotransformer.

Fig14 shows the results obtained for the proposed SC-48P system operating under normal conditions for the IPT #2 configuration. One can observe that AC line currents $i_{grid_a}$, $i_a$ and $i_{aut_a}$ for only phase A have THDs equal to 2.77%, 6.52% and 6.48% (meeting the IEEE-519 limits [24]), respectively. All of the amplitudes for the harmonics are mentioned. One can partially confirm that the IPT #1 and IPT #2 have good performance in terms of harmonic distortion, based on the results.

Furthermore, three scenarios were simulated for both IPTs arrangements to evaluate the performance of proposed SC-48P in degraded mode. Fig15 shows the results obtained for IPT #1. One can see that before instant $t = 1$ s, no faults were registered and the proposed SC-48P which operated effectively as a 48-pulse converter system. In this case, the THD value obtained for AC line current $i_{grid_a}$ is equal to the value presented in Fig. 13b. At instant $t = 1$ s and $t = 2$ s, scenario 2 is performed and the proposed SC-48P operates as a 24-pulse system, and the THD of current $i_{grid_a}$ is equal to 6.15%. At instant $t = 2$ s, scenario 3 kicks in. Here, the proposed SC-48P operates as a 12-pulse converter system and the THD of current $i_{grid_a}$ is equal to 13.21%.

Fig 16 shows the results obtained for the proposed SC-48P operating in degraded mode for the IPT #2. One should also observe that the SC-48P can efficiently operate as a 24-pulse and 12-pulse converter system, with THD levels of AC current $i_{grid_a}$ equal to 6.18% and 13.26% (values that are slightly smaller than those obtained for the IPT #1), respectively. We emphasize that all of the obtained values for the THD current in the AC power grid of the SC-48P operating

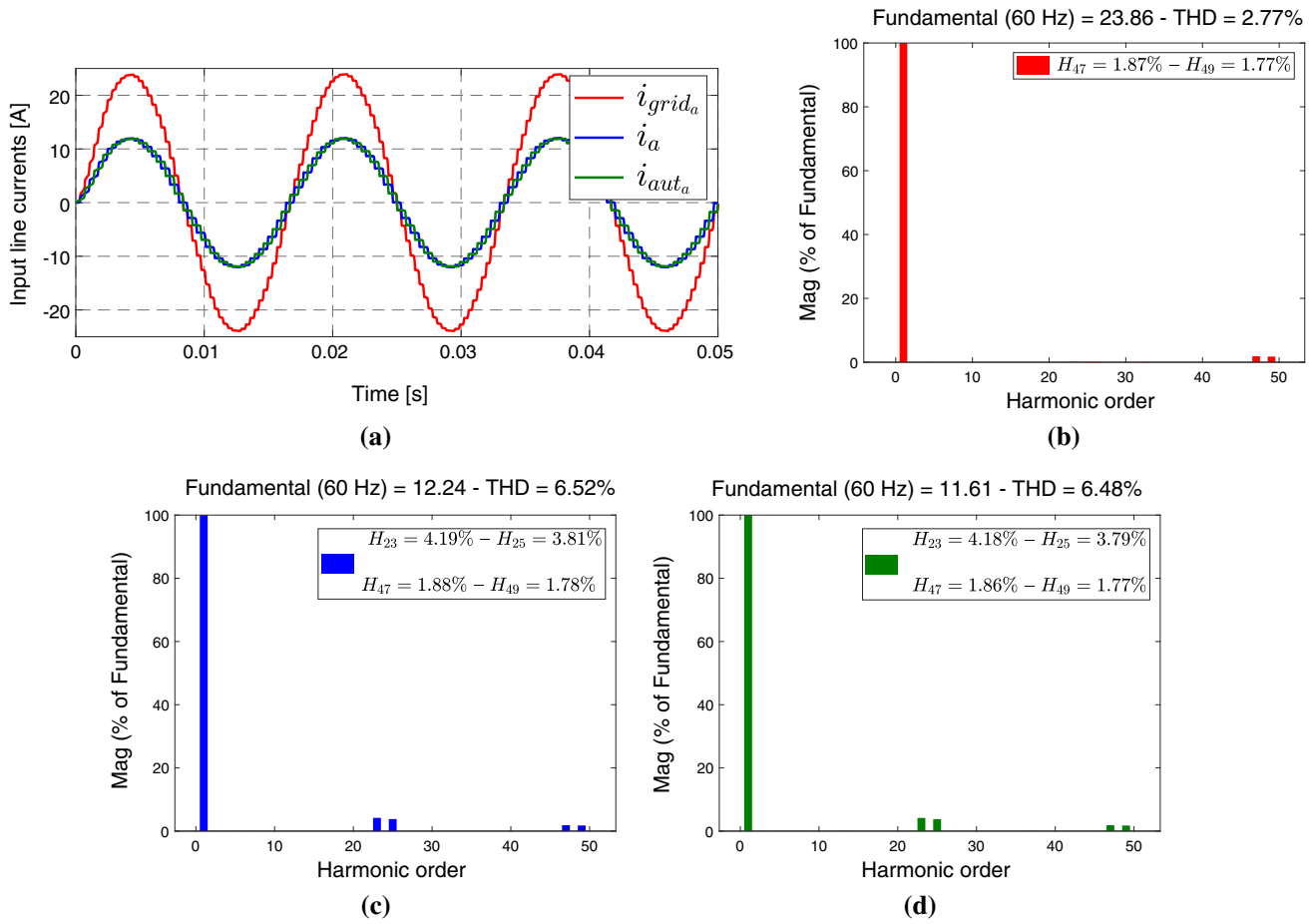


**Fig. 14** Simulation results of the proposed SC-48P operating under normal conditions for IPT #2. **a** Waveforms of AC line currents $i_{grid_a}$, $i_a$ and $i_{aut_a}$. **b**, **c** and **d** Harmonic spectrum of currents $i_{grid_a}$, $i_a$ and $i_{aut_a}$, respectively

in degraded mode for both IPTs meet IEEE-519 standards [24].

It should be noted effectively the presence of the $h = 24 \cdot k \pm 1, k \in \mathbb{Z}_+$ characteristic harmonics in AC line current $i_{grid_a}$ (Figs. 15b and 16b) when the proposed SC-48P is operating as a 24-pulse converter, and the presence of the $h = 12 \cdot k \pm 1, k \in \mathbb{Z}_+$ characteristic harmonics in AC grid current (Figs. 15c and 16c) when the proposed SC-48P system is working as a 12-pulse converter. Therefore, it also possible to conclude once more that the IPT #1 and IPT #2 perform satisfactorily in terms of the harmonic distortion and power quality improvements.

## 7 Experimental validation of the proposed SC-48P converter for IPT #2 configuration

To validate the aforementioned theoretical and simulations analysis and to prove the viability and applicability of the SC-48P prototype for industrial applications, we implemented experimental tests under normal operational conditions using only the IPT #2 configuration, due to the limitations of laboratory resources. The DC load for the R-L power applied was equal to 2.978 kW. The equipment parameters used in the tests are listed in Table 1. Measurements were taken using the Fluke 435 Power Quality Analyzer. Fig 17 shows the general view of experimental setup of proposed SC-48P converter.

Fig18 shows the experimental results obtained from the tests for the AC line currents $i_{grid_a}$, $i_a$ and their respective harmonic content. One can see that the THD value for currents $i_{grid_a}$, $i_a$ was equal to 2.9% and 5.2%, respectively, and the profile of the AC current in the electrical grid of the proposed SC-48P forms a practically sinusoidal wave.

Fig 19 shows the waveform of the input AC line current $i_{aut_a}$ of the autotransformer, its harmonic spectrum and the DC voltage for the R-L load. Note that the THD experimental value obtained for current $i_{aut_a}$ was equal to 3.3%. We emphasize that the obtained experimental THD values for AC line currents $i_{grid_a}$, $i_a$ and $i_{aut_a}$ are practically equal to those obtained in the simulations and are shown in Fig. 14b, c, d. From Fig. 18e, the active input power ($P_{in}$) associated with the proposed system considering the three phases is 3.004

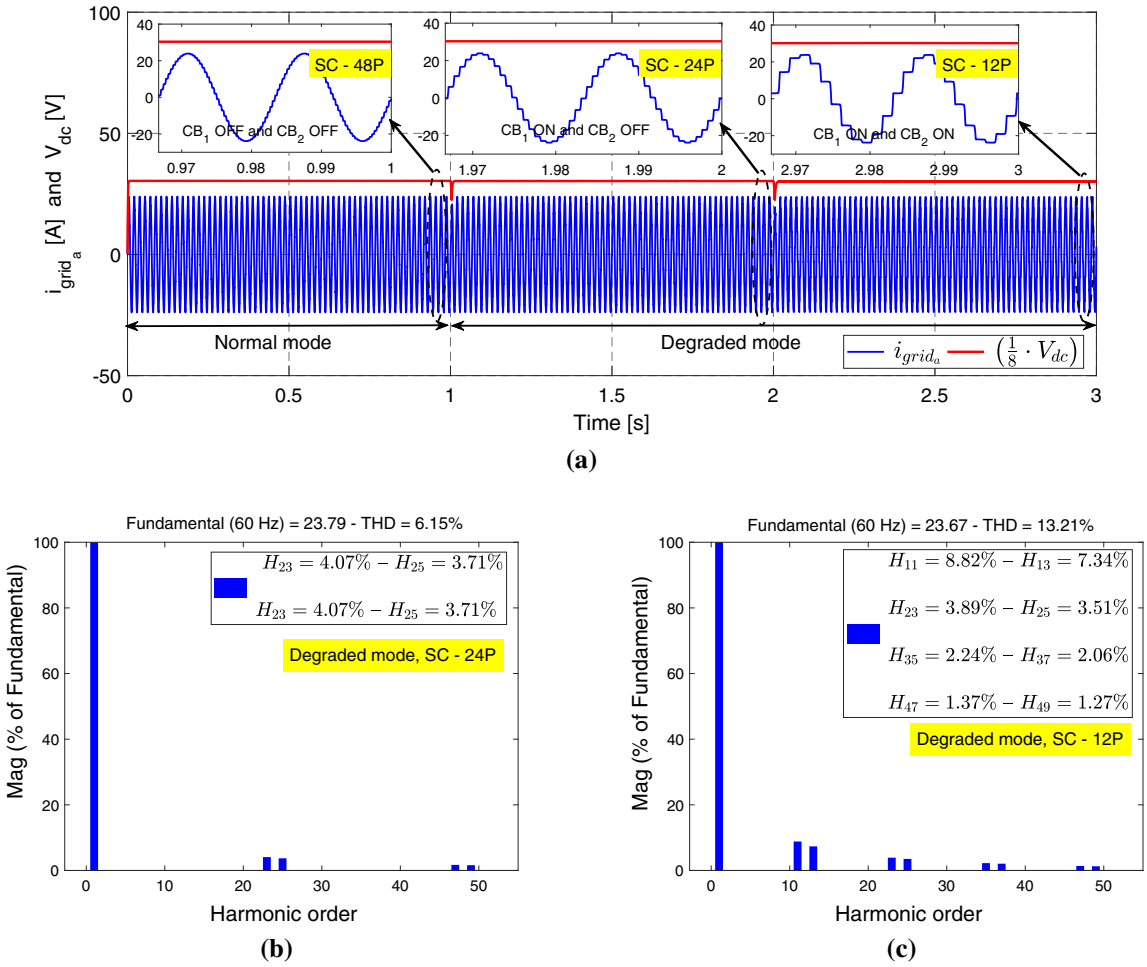


**Fig. 15** Simulation results for the proposed SC-48P operating in degraded mode for the IPT #1. **a** Waveform of AC current $i_{grid_a}$. **b** and **c** Harmonic spectrum of current $i_{grid_a}$, for scenarios 2 and 3. One-eighth of the DC voltage is displayed

**Table 2** Comparison of the proposed SC-48P scheme with other MPCs topologies

| Topologies | THD of AC current (%) | Load power | Reliability | Efficiency |
|---|---|---|---|---|
| 20-pulse [5] | 3.7 | 12 kW | Low | 97.65% |
| 12-pulse [7] | 12.5 | 12.045 kW | Low | –** |
| 40-pulse [8] | 4.3 | 7.5 kW | Low | 97.2% |
| 24-pulse [9] | 5.25 | 1 kW | Medium | –** |
| 24-pulse [11] | 3.9 | 1.92 kW | Medium | –** |
| 18-pulse [14] | 1.2 | 3 kW | Medium | –** |
| 12-pulse [12] | 1.3 | 6.4 kW | Low | 95.8% |
| 48-pulse [15] | 3.46 | 2.972 kW | Medium | 97.3% |
| SC-48P proposed | 2.9 | 2.978 kW | High | 99.13% |

** The authors of these papers did not present the value of the experimental efficiency

kW. Thus, the experimental efficiency $\left(\eta_{exp} = P_{out}/P_{in}\right)$ of the proposed SC-48P is found to be 99.13%, remembering that the applied DC load power is 2.978 kW due to laboratory limitations.

Table 2 reveals the comparison of the proposed converter with other MPCs in terms of input line current THD, load power, system reliability and efficiency. From Table 2, it is inferred that the high efficiency with improved power quality performances and high reliability of the proposed scheme are

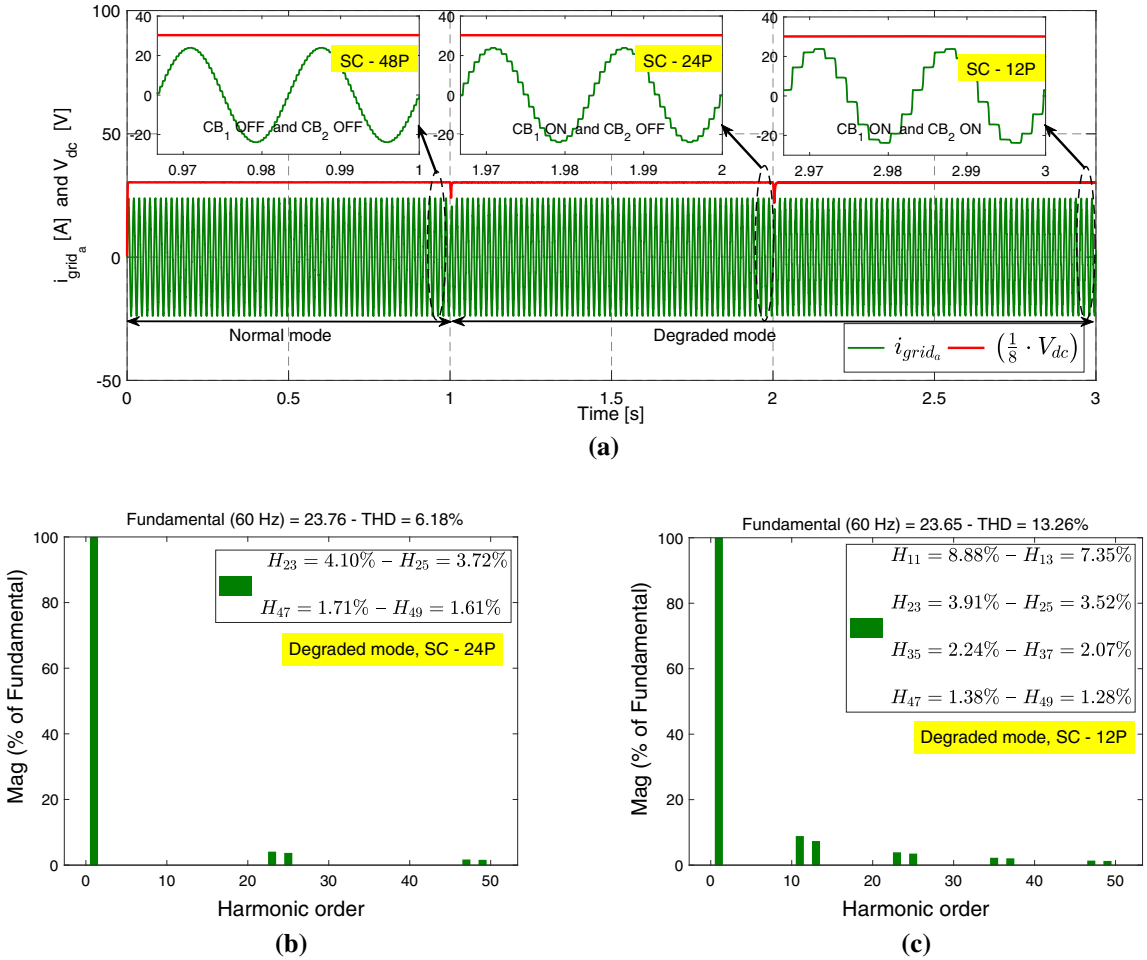


**Fig. 16** Simulation results for the proposed SC-48P operating in degraded mode for the IPT #2. **a** Waveform of AC current $i_{grid_a}$. **b** and **c** Harmonic spectrum of current $i_{grid_a}$, for scenarios 2 and 3. One-eighth of the DC voltage is displayed

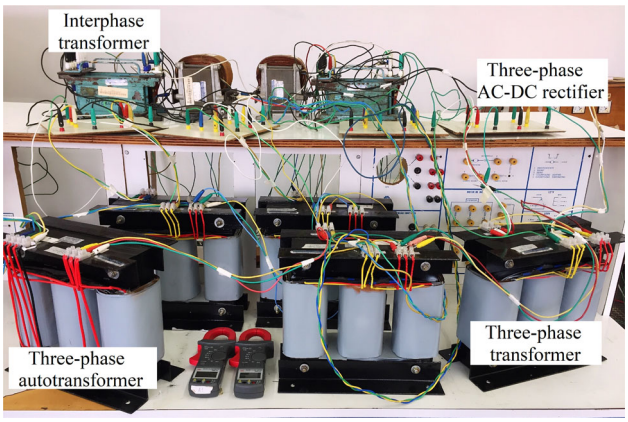


**Fig. 17** General view of experimental setup

the most commendable advantages of the proposed SC-48P as compared with other topologies.

On the other hand, based on Fig. 1, the unit cost of employed 4 kVA-220/220 V phase-shifting transformer and 2 kVA-220/180/180 V three-winding transformers is US$490.15 and US$379.75, respectively. Furthermore, the IPT #1 and IPT #2 transformer cost on the DC side of the proposed system amounts to US$788.50 and US$758.35, respectively. It is noteworthy that four (04) three-winding transformers are used in the SC-48P proposed. Therefore, the magnetic circuit total costs of the proposed system taking into account IPT #1 and IPT #2 arrangements are US$2797.65 and US$2767.50, respectively, according to the current quote.

From the results obtained, it is possible to confirm effectively the viability of the applicability of the proposed SC-48P scheme for use in industrial rectification, which can be extended to uses in the aluminum industry which requires currents in the range of hundreds of kiloamperes to be effective.

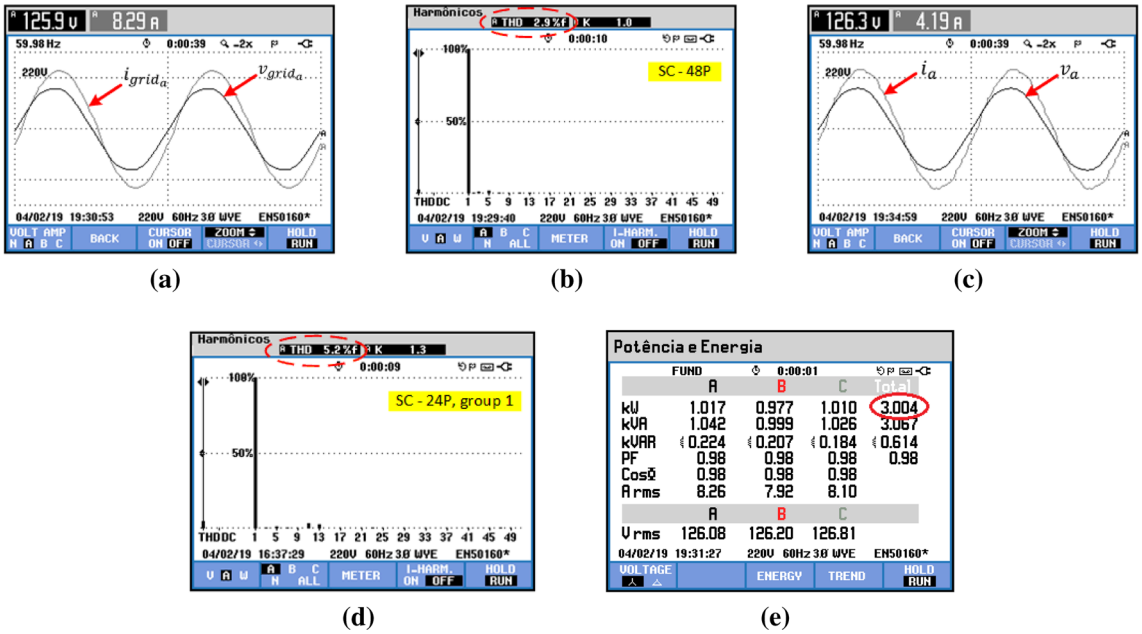


**Fig. 18** Experimental results for AC currents $i_{grid_a}$ and $i_a$. **a** and **c** Waveform of AC currents $i_{grid_a}$ and $i_a$. **b** and **d** Harmonic spectrum of line currents $i_{grid_a}$ and $i_a$. **e** Power parameters values

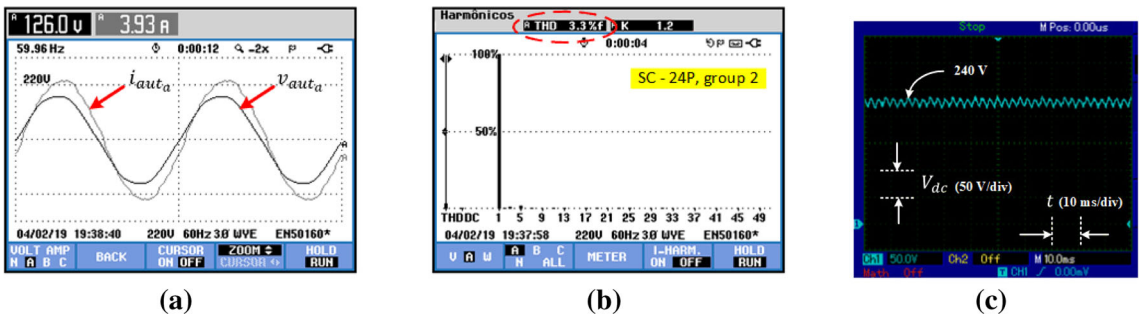


**Fig. 19** **a** and **c** Waveform of AC line current $i_{aut_a}$ and DC link voltage $V_{dc}$. (b) Harmonic spectrum of current $i_{aut_a}$. $time \rightarrow$ 10 ms/div and $V_{dc} \rightarrow$ 50 V/div

## 8 Conclusions

The proposed 48-pulse converter system, simulated and implemented, showed satisfactory performance in terms of harmonic distortion on the AC side of the power grid. The mathematical analysis of the AC line currents for the proposed SC-48P used as a method for calculation, estimating the inductance values of the IPT #1 and IPT #2, is presented in this paper.

Operating under normal conditions, the THD of the AC line current for the SC-48P was 2.75% and 2.77%, for IPT #1 and IPT #2, respectively, meeting the IEEE-519 requirements [24]. Furthermore, three scenarios were established in this paper to evaluate the reliability of the proposed SC-48P. The results derived from these evaluations confirm that the SC-48P can operate efficiently, in terms of reliability and power availability, as a SC-24P and SC-12P, depending on which faults may occur, i.e., when the proposed SC-48P operates as an SC-24P, the THD of the AC line current at mains is approximately 6.15% and 6.18%, for IPT #1 and IPT #2, respectively. When the proposed SC-48P operates as an SC-12P, the THD in the AC line current is 13.21% and 13.26% for IPT #1 and IPT #2, respectively. The results show that the IPT #1 and IPT #2 arrangements are efficient, in terms of the THD, under the same operational conditions (DC power equal to 6.4 kW). On the other hand, the experimental THD value under normal operating conditions was equal to 2.9%, only for IPT #2, which is close to the value predicted in the simulations. Furthermore, the simulated THD value for DC power equal to 2.978 kW for the IPT #2 was 3.014%, or very close to the experimental result obtained, which was 2.9%.

A phase-shifting autotransformer was inserted in the proposed topology for the arrangement of the second 24-pulse group. This group sees this autotransformer as a

series impedance in order to determine the effective overlap reactance of these four Graetz diode converter bridges. Remember that the percent impedance of the autotransformer is lower compared to the non-conventional transformer ones. As for the parallel association of converters, the greater the overlap reactance, the lower the contribution current of the converter; therefore, the inverse proportionality ratio occurs. The AC currents of the converter bridges of the second group are slightly smaller, thus occurring a slight imbalance in the AC line current distribution of the converters of the 48-pulse setup. This statement is experimentally verified in Figs. 18a and 19 a. This imbalance in the AC line current would be a disadvantage for the proposed system. An alternative solution to solve this problem would be inserting an autotransformer identical to the existing one at the input of the first group of the 24-pulse converter system, which would increase the system cost and physical space for high power special transformers. In this case, the tap values ($K_b$ and $K_c$) of the phase-shifting three-phase autotransformer calculated in Section. 3 for a displacement $\theta$ would need to be updated to obtain the proposed SC-48P effectively.

Based on the results, it is possible to confirm the viability and applicability of the proposed SC-48P for use in industrial applications since it presents consistent theoretical and experimental results, while a topology of this type has not yet been proposed in scientific literature. For future work, we intend to experimentally study the proposed SC-48P prototype using the IPT #1 configuration and compare the experimental results with those already obtained for the IPT #2 arrangement. Furthermore, we intend to make the didactic workbench for the proposed SC-48P more widely available for educational purposes, i.e., to use it in classes and lab experiments with undergraduate and graduate students alike, along with using it in training courses for industrial workers.

## Declarations

**Conflict of interest** The authors declare that they have no conflict of interest.

## References


1. Singh B, Gairola S, Singh BN, Chandra A, Al-Haddad K (2008) Multipulse AC-DC Converters for improving power quality: a review. IEEE Trans Power Electron 23:260–281. https://doi.org/10.1109/TPEL.2007.911880
2. Yang T, Bozhko S, Asher G (2014) Functional modeling of symmetrical multipulse autotransformer rectifier units for aerospace applications. IEEE Trans Power Electron 30:4704–4713. https://doi.org/10.1109/TPEL.2014.2364682
3. Solanki J, Fröhleke N, Böcker J, Averberg A, Wallmeier P (2015) High-current variable-voltage rectifiers: state of the art topologies. IET Power Electron 8:1068–1080. https://doi.org/10.1049/iet-pel.2014.0533
4. Gao L, Xu X, Man Z, Lee J (2018) A 36-pulse diode-bridge rectifier using dual passive harmonic reduction methods at dc link. IEEE Trans Power Electron 34:1216–1226. https://doi.org/10.1109/TPEL.2018.2835511
5. Kalpana R, Singh B, Bhuvaneswari G et al (2017) A 20-pulse asymmetric multiphase staggering autoconfigured transformer for power quality improvement. IEEE Trans Power Electron 33:917–925. https://doi.org/10.1109/TPEL.2017.2721958
6. Sandoval JJ, Krishnamoorthy HS, Enjeti PN, Choi S (2016) Reduced active switch front-end multipulse rectifier with medium-frequency transformer isolation. IEEE Trans Power Electron 32:7458–7468. https://doi.org/10.1109/TPEL.2016.2632717
7. Meng F, Gao L, Yang S, Yang W (2015) Effect of phase-shift angle on a delta-connected autotransformer applied to a 12-pulse rectifier. IEEE Trans Ind Electron 62:4678–4690. https://doi.org/10.1109/TIE.2015.2405058
8. Abdollahi R, Gharehpetian GB (2016) Inclusive design and implementation of novel 40-pulse AC-DC converter for retrofit applications and harmonic mitigation. IEEE Trans Ind Electron 63:667–677. https://doi.org/10.1109/TIE.2015.2481364
9. Yang S, Wang J, Yang W (2017) A novel 24-pulse diode rectifier with an auxiliary single-phase full-wave rectifier at dc side. IEEE Trans Power Electron 32:1885–1893. https://doi.org/10.1109/TPEL.2016.2560200
10. Kalpana R, Chethana KS, Singh B et al (2018) Power quality enhancement using current injection technique in a zigzag configured autotransformer-based 12-pulse rectifier. IEEE Trans Indus Appl 54:5267–5277. https://doi.org/10.1109/TIA.2018.2851566
11. Meng F, Xu X, Gao L (2017) A simple harmonic reduction method in multipulse rectifier using passive devices. IEEE Trans Indus Inform 13:2680–2692. https://doi.org/10.1109/TII.2017.2723602
12. Meng F, Yang W, Yang S, Gao L (2015) Active harmonic reduction for 12-pulse diode bridge rectifier at DC side with two-stage auxiliary circuit. IEEE Trans Indus Inform 11:64–73. https://doi.org/10.1109/TII.2014.2363522
13. Meng F, Xu X, Gao L, Man Z, Cai X (2018) Dual passive harmonic reduction at dc link of the double-star uncontrolled rectifier. IEEE Trans Indus Electron 66:3303–3309. https://doi.org/10.1109/TIE.2018.2844840
14. Young CM, Wu SF, Yeh WS, Yeh CW (2013) A DC-side current injection method for improving AC line condition applied in the 18-pulse converter system. IEEE Trans Indus Electron 29:99–109. https://doi.org/10.1109/TPEL.2013.2248067
15. Lian Y, Yang S, Yang W (2019) Optimum design of 48-pulse rectifier using unconventional interphase reactor. IEEE Access 7:61240–61250. https://doi.org/10.1109/ACCESS.2019.2902453
16. Wu B, Narimani M (2017) High-power converters and AC drives, 76–78. John Wiley & Sons, https://ieeexplore.ieee.org/book/7823162
17. Francis R, Meganathan D (2019) A dual-mode cascaded H-bridge multilevel inverter for improving THD. Elect Eng 101:225–237. https://doi.org/10.1007/s00202-019-00768-y
18. Kunzler LM, Lopes LAC (2021) A novel algorithm for increased power balance in cascaded H-bridge multilevel cells in a hybrid power amplifier. Elect Eng 103:551–562. https://doi.org/10.1007/s00202-020-01102-7
19. Ogoulola CEG, Rezek AJJ, Fifatin F et al (2020) An alternative proposal for HVDC transmission systems using 24-pulse AC/DC converters based on three-winding non-conventional transformers. Electric Power Syst Res 182:106230–106240. https://doi.org/10.1016/j.epsr.2020.106230
20. Rezek AJJ, Ogoulola CEG, de Abreu JP, et al., (2016) Winding turns calculus methodology for a new 48 pulse multiconverter system employing lower cost three winding special transform-

ers, 17th International Conference on Harmonics and Quality of Power (ICHQP). IEEE, 18–23. https://doi.org/10.1109/ICHQP.2016.7783414
21. Williams BW (2006) Principles and elements of power electronics, 456–458. Devices, Drivers, Applications and Passive Components, http://personal.strath.ac.uk/barry.williams/book.htm
22. Sefa I, Altin N (2009) A novel approach to determine the interphase transformer inductance of 18 pulse rectifiers. Energy Conv Manag 50:2495–2503. https://doi.org/10.1016/j.enconman.2009.05.015
23. Monroy AO (2013) Study of polyphase rectifier circuits with suitable performance for power network of aircrafts (in French). Master dissertation, Laval University. http://hdl.handle.net/20.500.11794/24252
24. Duffey CK, Stratford RP (1989) Update of harmonic standard IEEE-519: IEEE recommended practices and requirements for harmonic control in electric power systems. IEEE Trans Indus Appl 25:1025–1034. https://doi.org/10.1109/PCICON.1988.22445